4-4-2018

Multi-point Vibration Measurement and Mode Magnification of Civil Structures using Video-based Motion Processing

Zhexiong Shang
University of Nebraska-Lincoln, zshang@unomaha.edu

Zhigang Shen
University of Nebraska - Lincoln, shen@unl.edu

Multi-point Vibration Measurement and Mode Magnification of Civil Structures using Video-based Motion Processing

Zhexiong Shang, Zhigang Shen*

The Durham School of Architectural Engineering and Construction, College of Engineering, University of Nebraska-Lincoln, 113 NH, Lincoln, NE 68588, USA

* Corresponding author. email address: shen@unl.edu

Abstract

Image-based vibration measurement has gained increased attentions in civil and construction communities. A recent video-based motion magnification method was developed to measure and visualize small structure motions. This new approach presents a potential for low-cost vibration measurement and mode shape identification. Pilot studies using this approach on simple rigid body structures were reported. Its validity on complex outdoor structures have not been investigated. In this study, a non-contact video-based approach for multi-point vibration measurement and mode magnification is introduced. the proposed approach can output a full-field vibration map where the structural potential anomaly can be identified. The proposed multi-point approach is developed based on the local phases which also fills the gap of the existing intensity-based multi-point vibration measurement. As an extension of the phase-based motion magnification, the multi-point measurement result is then integrated with the maximum likelihood estimation (MLE) to estimated the magnified frequency bands at each identified structure mode for operational deflection shape (ODS) visualization. This proposed method was tested in both indoor and outdoor environments for validation. The results show that with the developed method, mode frequencies of complex structures are simultaneously measured and mode shapes of each structure are automatically visualized.

Keywords

Video-based Vibration Measurement; Phase-based Optical Flow; Motion Magnification; Mode Identification; Operation Deflection Shape

Highlights

1. Develops a non-contact video-based approach for multi-point vibration measurement and mode magnification using the phase-based optical flow

2. Able to generate pixel-wise full-field vibration map for structural anomaly detection

3. Estimate the amplified frequency bands for motion magnification without human intervention

4. Employ the proposed approach on in-service complex civil structures

1. Introduction

In the last decades, vibration-based modal analysis was one of the most widely used techniques in structural health monitoring (SHM) of civil infrastructures. The fundamental idea is that the damage, aging and environmental-induced deterioration will result in the change of the physical properties of structures (e.g. mass, damping and stiffness) that can be detected by measuring the abnormal responses of structural vibration [1]. Current vibration measurement can be classified as contact and non-contact methods. The contact method requires engineers to manually instrument contact transducers, such as linear variable displacement transducers (LVDT), accelerometers or strain gages, at locations of interest to observe the amplitudes and frequencies of structural oscillations [2]. The contact sensors can detect vibrations at high accuracy and long dynamic ranges, however, the physical installation process is cumbersome, and added mass of loadings may also change the natural behaviors of the lightweight inspection targets that limits the practicability of this method in many disciplines [3]. Such limitations can be attenuated by using the non-contact measurement approaches. Currently, the most widely used non-contact sensors includes Laser Doppler Vibrometry (LDV), synthetic aperture radar (SAR), ultra-sound and vision system. The vision system relies on camcorder to record time series image sequence which has the advantages of low-cost, texture rich and easy to implement. With the recent development of image processing and computer vision techniques, the accuracy and robustness of the vision-based approach has been greatly improved which make it applicable for field measurements [4].

Tracking algorithm is one of the most widely used vision approaches for vibration measurement. It relies on edge detection, digital image correlation (DIC), pattern matching or object recognition to extract features in each image, and measures the displacements by counting the movements of these features in pixels over time [5-7]. The existing studies used feature-rich markers mounted on the inspection targets to measure the vibration of in-service structures [8, 9]. Due to the size and geometry of the markers are known, the structural displacements were estimated by directly tracking the movements of these markers. However, the markers still need to be manually placed on the hard-to-reach parts of a structure, the convenience of using such non-contact method is reduced. Recent study suggested that by using objects' own features, marker-less approaches can reach similar level of accuracy as the marker approach for field applications [10]. For example, the bridge decks, cables, beams and hangers always show high gradient in textures where the displacements can be measured by tracking these features over time [11, 12]. The tracking method has the advantages of direct displacement measurement, however, it requires notable structural motions at feature points. Motions without apparent pixel-level changes make the method unsuitable, which is the major drawback of this method.

Comparing to the tracking method, optical flow can achieve sub-pixel accuracy by estimating the apparent velocity of movements in images. The method assumed that the image illuminations are constant and all intensity variations are linearly related to the motions of objects [13]. The existing study showed that optical flow can monitor the sub-pixel vibrations even for long distance measurement [14]. Recently, a technique called virtual visual sensor (VVS), which follows the same assumption as optical flow, was developed [15]. The method is able to efficiently capture the vibration frequency by counting the intensity changes at each pixel [16]. However, without in-plane reference, such method fails to estimate the magnitude of structural vibration because no

direct connection has been found between the pixel luminosity changes and vibration amplitudes [17].

Lately, researchers in Massachusetts Institute of Technology (MIT) introduced a novel yet simple approach, called Eulerian video magnification, to magnify subtle motions in a video so they can be perceptible to naked eyes [18]. The method multiples a magnification factor with the intensity value change to amplify the motions in the video. However, simply amplifying the intensity variations will also increase the noise powers that results in artificial results in the reconstructed video. To reduce this noise floor, a phase-based motion magnification method was developed which uses local phases to encode the temporal motions [19]. Compare to the intensity strength, motion estimated by phases is more robust to environmental noise, such as the image illumination, perspective and surface pattern changes [20].

In [21, 22], Chen et al applied the noncontact phase-based optical flow to measure the vibrations of simple laboratory-scale structures. The measured vibration peaks are then used to identify the frequency bands of motion magnification such that the operating deflection shapes (ODS) of these structures are visualized. [23] evaluated the accuracy of the phase-based optical flow by comparing it with other traditional vibration measurement approaches. The study validated the algorithm's sub-pixel accuracy and concluded that the best result is highly dependent on the selection of active pixels and the levels of subsampling. In [24], the phase-based method was integrated with blind source separation (BBS) technique to automatically identify modal parameters (e.g. frequency, stiffness, damping ratio). The method combined the principle component analysis (PCA) with complex pursuit (CP) to extract the active mode shapes of laboratory scale structures without human interaction. To investigate the feasibility of the motion magnification on structural anomaly detection, an experiment was carried out in [25] where the damaged WTB was identified by comparing the ODS vectors with a baseline WTB using the Model Assurance Criterion (MAC).

Up to now, the existing studies showed the potentials of using the phase-based method to measure the dynamic response and visualize the vibration modes of simple benchmark structures. However, its application on complex in-service civil structures is still missing. In practice, the in-service civil infrastructures, such as steel bridges, are composed of hundreds or thousands of substructures while each one of them may present distinct vibration responses under excitations. Thus, being able to identify the dynamic responses and efficiently visualize the ODS of multiple targets in the scene are critical to increase the practicability of the current phase-based motion magnification on SHM applications.

In this study, a non-contact video-based multi-point vibration measurement approach using the phase-based optical flow is introduced. The method outputs a full-field vibration map in which the resonance frequencies measured at each active pixel are color coded for potential anomaly detection. Comparing to the existing multi-point methods which relies on intensity levels change [26], the proposed method fills the gaps by using the local phases which is more robust to environmental noises. As an extension of the phase-based motion magnification on SHM, this study investigated the potentials of applying motion magnification on complex in-service civil structures. To acquire better visualization result with least human intervention, a non-parametric method is applied to estimate the interested frequency bands for vibration mode magnification using the maximum likelihood estimation (MLE). The proposed method is both tested on a

benchmark cantilever beam in laboratory environment and in-service steel bridges in the fields for validation.

2. Method

Figure 1 presents the general workflow of the proposed multi-point vibration measurement approach. It is consisted of four major steps: images pre-processing, phase-based optical flow, noise reduction and mode magnification. The details of each step of are fully discussed in the followings.

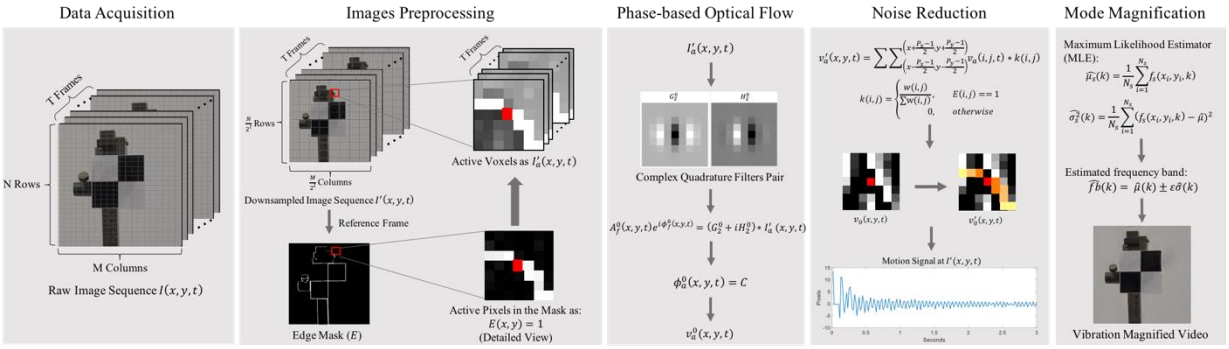

Figure 1 Semantic Diagram of the Proposed Method

2.1 Images Pre-processing

A time series of images (e.g. video) with structures of interest in the scene is taken as the input of this method. The raw image sequence is firstly subsampled with Gaussian pyramids to reduce the white noise. The selected levels of subsampling must be determined based on the spatial resolution of the raw image sequence, in most cases, the times of down sampling should equal or less than four [23]. An edge mask is then processed on a reference frame to extract the high contrast regions in the scene. Many edge detection algorithms can be applied to generated the mask, in this study, the authors use the amplitude, which is the byproduct of the phase-based optical flow, with a pre-defined threshold to generate the mask. There are several benefits of using the edge mask: First, it helps reduce the number of pixels needs to be processed. For example, a normal 700×700 grayscale image contains 490,000 pixels while the number of pixels at high contrast regions can shrink to 2000 to 8000. Second, it helps removes the weak feature points as the motion signals estimated by phase does not meaningful at low amplitude regions. After the images pre-processing, the phase-based optical flow is applied on each pixel in the mask. In the following, the authors use the active pixels to define the pixels extracted from the mask.

2.2 Phase-based Optical Flow

The phase-based optical flow was developed based on the assumption that brightness in the scene remains unchanged, and the temporal variation of image intensity was due solely to the image translations[20, 27]. In Fourier transform, the phase controls the global location of basis function while the amplitude defines the strengths. The local motion can be estimated by shifting the local

phase, which is computed as a Gaussian window multiplied by a complex sinusoid function [19]. To identify the local phases in images, the phase-based method spatially convolves the frames through a complex bandpass filter [28]. In this study, the complex steerable quadrature filters pair ($G_2^\theta + iH_2^\theta$) applied in [22] is used as the kernel function where the real part is the frequency response of the second derivative of a Gaussian (G_2), the imaginary part is its Hilbert transform (H_2), and the θ presents the orientation of phase shift in radiance [15, 16]. Let $I(x, y, t)$ represents a grayscale image sequence where x and y are Cartesian coordinates and t denotes the time stamps. The local phase (ϕ) and local amplitude (A) at orientation θ can be computed as in Equation (1):

$$A_\theta(x, y, t)e^{i\phi_\theta(x,y,t)} = \left(G_2^\theta + iH_2^\theta\right) * I(x, y, t) \tag{1}$$

Figure 2 shows an example of amplitude and phase images with $\theta = 0$ and $\theta = {}^{\pi}/_{2}$. Due to the constant phase contour can estimate temporal motions, the local phases are then used to calculate the velocity in units of pixels by computing the derivative of the phase in both spatial and temporal domains. The formula of image velocity estimated by local phase is illustrated in Equation (2).

$$\begin{aligned} v_0(t) &= -\left(\frac{\partial \phi_0(x, y, t)}{\partial x}\right)^{-1} \frac{\partial \phi_0(x, y, t)}{\partial t} \\ v_{\pi/2}(t) &= -\left(\frac{\partial \phi_{\pi/2}(x, y, t)}{\partial y}\right)^{-1} \frac{\partial \phi_{\pi/2}(x, y, t)}{\partial t} \end{aligned} \tag{2}$$

where $v_0(t)$ and $v_{\pi/2}(t)$ respectively denote the image velocities in x ($\theta = 0$) and y ($\theta = {}^{\pi}/_{2}$) directions at time t. The computed velocities are then integrated over time to obtain the in-plane displacements. Without considering the image distortion, the displacement of units of pixel can be converted to engineering unit (e.g. millimeters) by multiplying a scaling factor.

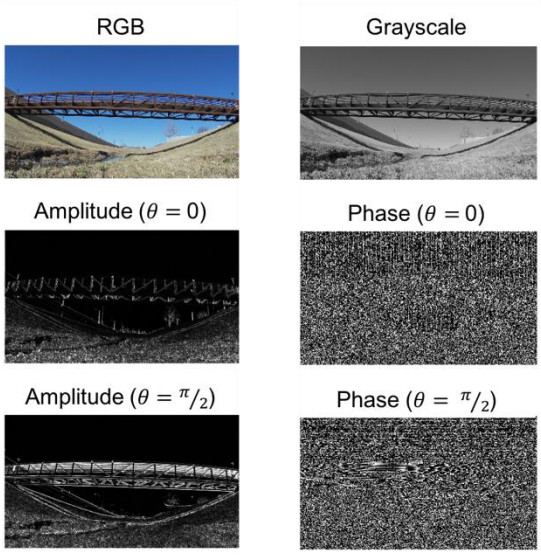

Figure 2 Amplitude and phase images with $\theta = 0$ and $\theta = \pi/2$

2.3 Noise Reduction

Although motion estimated at each active pixel is valid, it is still sensitive to the intrinsic and extrinsic parameters, such as spatial resolution, edge strength and illumination changes. In the original phase-based method, the noisy signals were handled with a pixel-wise amplitude-weighted blur [22]. This method can increase the signal's SNR, while it is not capable of describing the motions at each location accurately as the signals may shift to the neighbors with large amplitudes. To overcome this problem, a mask-based kernel is designed such that the information close to target pixel are enhanced while the others are attenuated. Due to the phase-based signals is not meaningful at low amplitude regions, only active pixels defined in the edge mask are used. The proposed mask-based kernel is initially defined as a symmetrical filter with weight coefficients linearly related to the inverse of the distance from the target pixel. Then, the kernel is remapped to unit by dividing its sum only at local active pixels. Equation (3) presents the noise reduction process using the mask-based kernel (k):

$$v'(x,y,t) = \sum\sum_{(x-\frac{P_x-1}{2},y-\frac{P_y-1}{2})}^{(x+\frac{P_x-1}{2},y+\frac{P_y-1}{2})} v(i,j,t) * k(i,j) \tag{3}$$

$$k(i,j) = \begin{cases} \dfrac{w(i,j)}{\sum w(i,j)}, & E(i,j) = 1 \\ 0, & otherwise \end{cases}$$

where v and v' respectively indicates the motion signals at $I(x,y,t)$ before and after the noise reduction. P_x, P_y are the row and column size of the mask-based kernel with center at $(x,y), and$ $w(i,j)$ is the initial weight coefficients of the linear filter. In this study, the authors normalize the rows of Pascal's triangle [29] to estimate the initial weights in the filter. A semantic comparison of the weight coefficients with and without weight remapping using the proposed mask-based

kernel is shown in Figure 3. For field measurement, these spatially blurred motion signals are then temporally processed with a Gaussian filter to reduce the noise caused by the illumination changes. The computed signals are then transferred into frequency spectrum using the Discrete Fourier transform (DFT) and the resonant frequencies can be identified with peak picking or frequency domain decomposition (FDD) [30]. The identified resonant frequencies at each active pixel can generate a full-field vibration map such that the dynamic response at different locations are simultaneously identified.

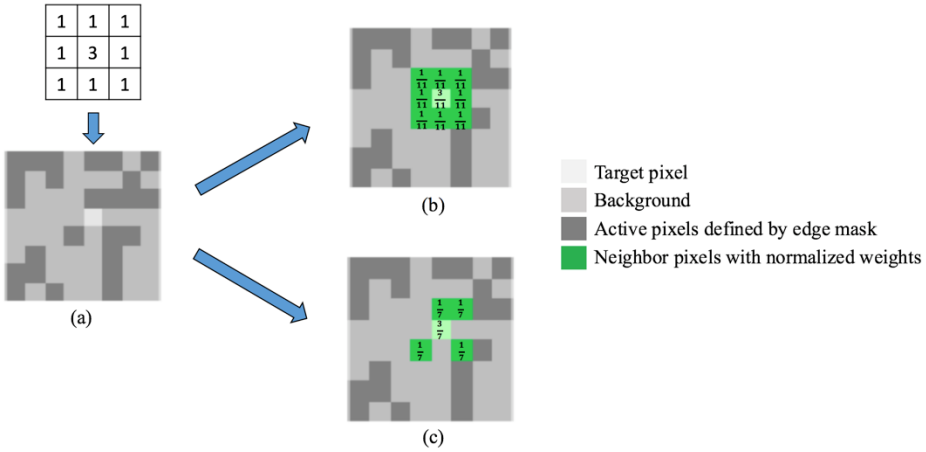

Figure 3 (a) Original Image with a 3 × 3 linear filter convolved on a target pixel; (b) Normalized weight coefficients at neighbor pixels without using mask-based kernel; (c) Remapped weight coefficients with the proposed mask-based kernel

2.4 Mode Magnification

Modal analysis includes both the modal frequency and mode shapes [14]. The existing studies showed that the motion magnification can be applied as a tool to visualize the structures' operational deflection shape (ODS) [21]. It relies on temporal filters to manipulate phase variations under a specific frequency band and magnifies it for mode visualization. However, current motion magnification requires users to manually select the amplified frequency bands, which is neither effective nor applicable for complex structures. Thus, in this section, a non-parametric method is introduced to efficiently identify the frequency bands without human interaction. The method is developed based on the assumption that simple structure shows uniform dynamic response and the major contributor of measurement error is the white noise [27]. Therefore, motions at each structure must follow the Gaussian distribution with certain mean (μ) and variance (σ^2). In this study, the Maximum Likelihood Estimation (MLE) is applied to estimate the true value of these parameters. Given the vibration frequencies of active pixels on a target structure as input, the maximum likelihood estimator of the mean (μ) and variance (σ^2) can be identified by solving the equation of partial derivatives of logarithm of MLE [31]. The estimated mean ($\hat{\mu}$) and variance ($\widehat{\sigma^2}$) using MLE at structure (s) are illustrated in Equation (4).

$$\hat{\mu}_s(k) = \frac{1}{N_s}\sum_{i=1}^{N_s} f_s(x_i, y_i, k)$$

$$\widehat{\sigma^2}_s(k) = \frac{1}{N_s}\sum_{i=1}^{N_s} (f_s(x_i, y_i, k) - \hat{\mu})^2 \quad (4)$$

where $f_s(x_i, y_i, k)$ is the kth strongest frequency peak located at pixel $I(x_i, y_i)$ that belongs to structure s in the scene, and N_s is the number of $f_s(x_i, y_i, k)$ on s. Based on the computed $(\hat{\mu}, \widehat{\sigma^2})$, the estimated frequency band $(\widehat{fb})$ can be determined as in Equation (5):

$$\widehat{fb}(k) = \hat{\mu}(k) \pm \varepsilon * \hat{\sigma}(k) \quad (5)$$

where ε is a user defined constant. There are two criteria to define the ε: 1) Each band must cover and only cover a single frequency peak as band cover a mixture of resonant frequencies fail to demonstrate the real mode shapes. 2) ε should be kept small as a narrow band can always achieve better visualization results. In this study, the authors iteratively picking the strongest peaks in decreasing order and set the ε for each band such that no band is overlapped with other peaks. To minimize the possibility of selecting spurious peaks, instead of searching the entire frequency spectrum, a local search region with center located at $\hat{\mu}$ can be preempted. Compare to the deterministic methods, finding the frequency band with probabilistic technique enhances the estimator's robustness to noises and outliers. These identified bands are then used as the input of motion magnification to reconstruct the vibration amplified video. This non-parametric progress can be parallel processed to simultaneously visualize the ODS of multiple interested structures.

3. Experiments

In this section, the method is validated through both indoor laboratory test and outdoor field measurements. The details of experimental setup, parameter configuration and the test results are described below.

3.1 Laboratory Experiment

Motions estimated with the proposed phase-based optical flow are initially validated on a benchmark cantilever beam at an indoor laboratory environment. A paper printed 2 × 2 checkerboard is attached on the beam to increase its geometric complexity. A hammer strikes at the free end of the beam that gives it an impulse for horizontal vibration. The video of the vibration is captured by a tripod stabilized consumer grade camera localized 1.2 meters away from the beam with camera lens perpendicular to the center of the marker. The camera is set at the high frequency mode with resolution at 1920×1080 and frame rate at 240 fps. It should be noticed that the spatial resolution of the image sequence cannot be too low after the subsampling, which may generate inaccurate results [23]. An accelerometer is mounted behind the center of the marker to record the ground-truth data at the sampling rate of 400 Hz. Figure 4 (a) presents the data acquisition process of the indoor experiment.

The raw image sequence is cropped to focus on the vibrating beam and downsampled twice for computation efficiency. Three individual pixels P1, P2 and P3 (respectively marked as triangle, circle and cross in Figure 4(b)) located at the active pixels are manually selected and processed through the proposed method. Due to the high spatial resolution of the image, a 5×5 kernel is applied for noise reduction. The computed motion signals in pixels are then converted into millimeters using the pinhole camera model by scaling the width of the marker in real world with it in images. Figure 5 demonstrates the synchronized displacement signals in millimeters with both camera and accelerometer at temporal and frequency domains. The averaged normalized root mean square error (NRMSE) of the camera measured displacement signals is smaller than 0.1%, which verifies the accuracy of the proposed algorithm.

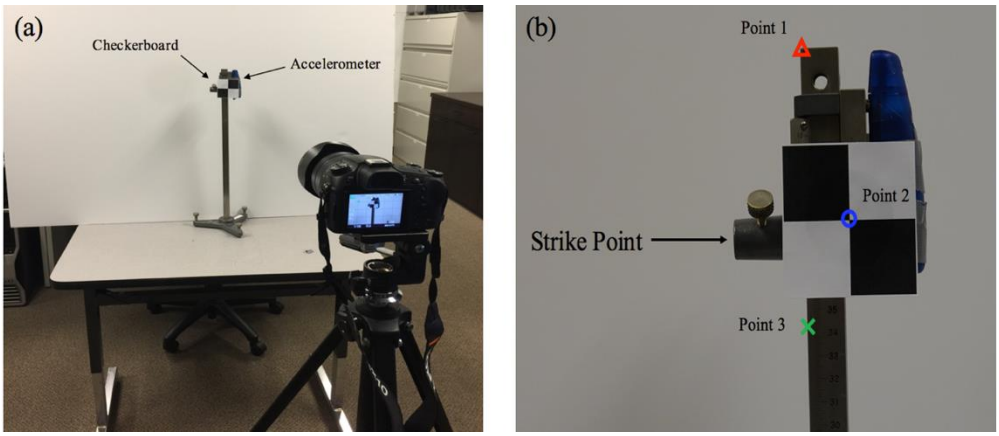

Figure 4 (a). The laboratory experiment setup; (b). Cropped camera view of vibration measurement, the striking point and the selected validation points are presented

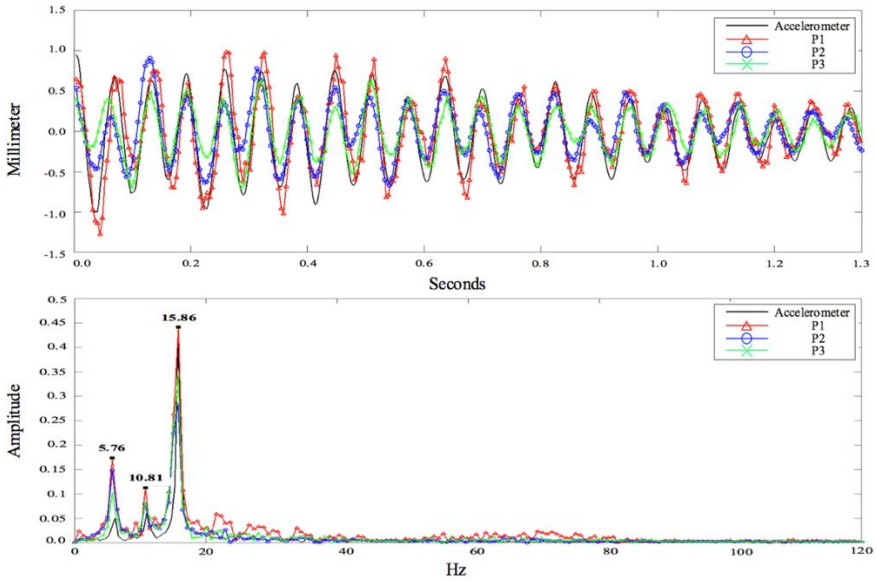

Figure 5 Horizontal displacement signals of camera and accelerometer. Top: displacement signals in time domain; Bottom: displacement signals in frequency spectra

After the result of individual pixels have been validated, the authors detached the accelerometer to reflect the natural behavior of the entire beam. The same experimental setup is applied and, at this time, vibration measurement is applied on the entire scene. The initial frame is selected as the reference with edge mask threshold set as the median of all local amplitudes in the frame. Figure 6 presents the color-coded vibration map of resonant frequencies computed at each active pixel. It can be visualized that the entire structure shows similar results close to the computed 3rd mode (shown in Figure 5) under the variation of ± 0.3 Hz. Such minor difference may result from the revolute joint located behind the marker that causes a slightly different response under excitation. Although the proposed method can produce full field map of the strongest peak (the 3rd mode), due to the sharply dropped SNR, it fails to generate valid results for the non-strongest peaks (1st and 2nd modes) where the spurious peaks and outliers that may not belong to any identified modes will be appeared in the map. Such limitation can be potentially mitigated by considering the spatial topology of active pixels which will be explored in the future study.

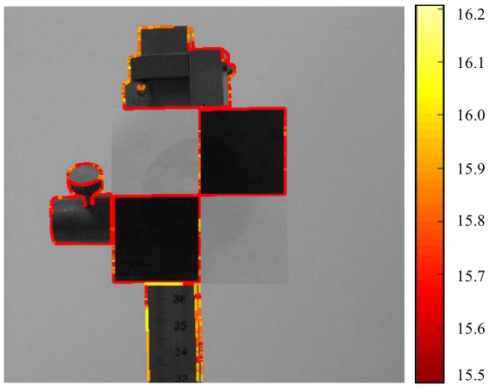

Figure 6 Color coded vibration map at all active pixels in the camera view, the color bar indicates the scale of frequency at each pixel.

3.2 Field Measurement

Pedestrian Bridge

In this section, an experiment is carried out at an outdoor in-service pedestrian bridge (in Figure 7). The bridge is 41.5 meters long and 3.66 meters wide, active loading on this bridge is produced by people jumping at its mid-span. Two accelerometers are mounted near the jump location with frame rate at 256 fps. A consumer-grade video camera is set 15 meters away from the bridge to measure the vertical vibrations. Based on the Nyquist-Shannon sampling theorem that the sampling rate needs to be set to at least twice of the highest anticipated frequency to be distinguishable in the signal [18] and most bridge resonant vibration frequencies are under 5 Hz, a camcorder setup at the resolution of 1080×920 and frame rate of 60 fps is sufficient for displacement extraction. The video's duration is nearly 17 seconds long with nearly 1000 frames captured. The proposed method is not affected by air temperature and humidity. However, other environment conditions, such as wind-induced camera vibration and illumination change, may cause serious problems. Therefore, a sunny data with no clouds and wind speed smaller than 5 mph is selected for data collection. The camera support and wind shield should be also utilized to minimize the measurement errors. Due to the phase-based motion estimation is highly dependent

on the image contrasts, it is always recommended to set up a camera view where there is a high contrast between the target and background.

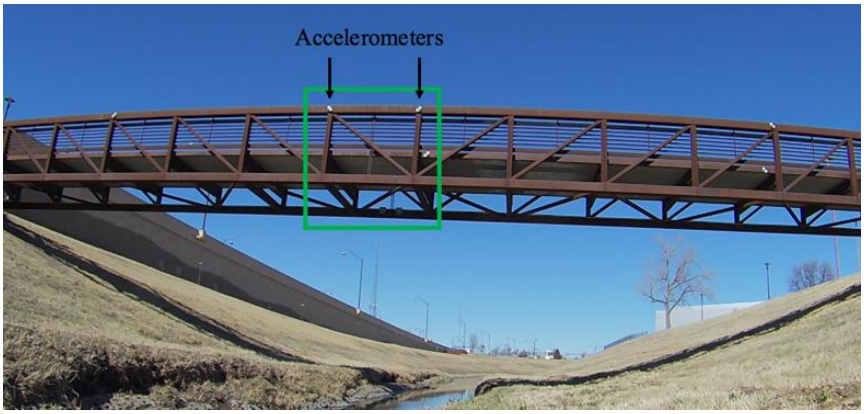

Figure 7 The pedestrian bridge, locations of accelerometers and the cropped camera view (green rectangle)

The image sequence is pre-cropped to focus on the mid-span of the bridge (as shown in green rectangle in Figure 7). Due to the low spatial resolution of the images and the high structural complexity, the cropped images are downsampled only once and the selected kernel size for noise reduction is 3×3. To validate the accuracy of the proposed method, a small region of interest (ROI) as shown in Figure 9 (a) is pre-selected, and the displacements at each active pixel within the ROI are averaged and compared with the accelerometers. Figure 8 shows the camera measured sub-pixel displacements and its comparison with the accelerometers in frequency domain. The result shows that the errors of all four modes are under 4% which indicated a high accuracy of the proposed method even under outdoor environment.

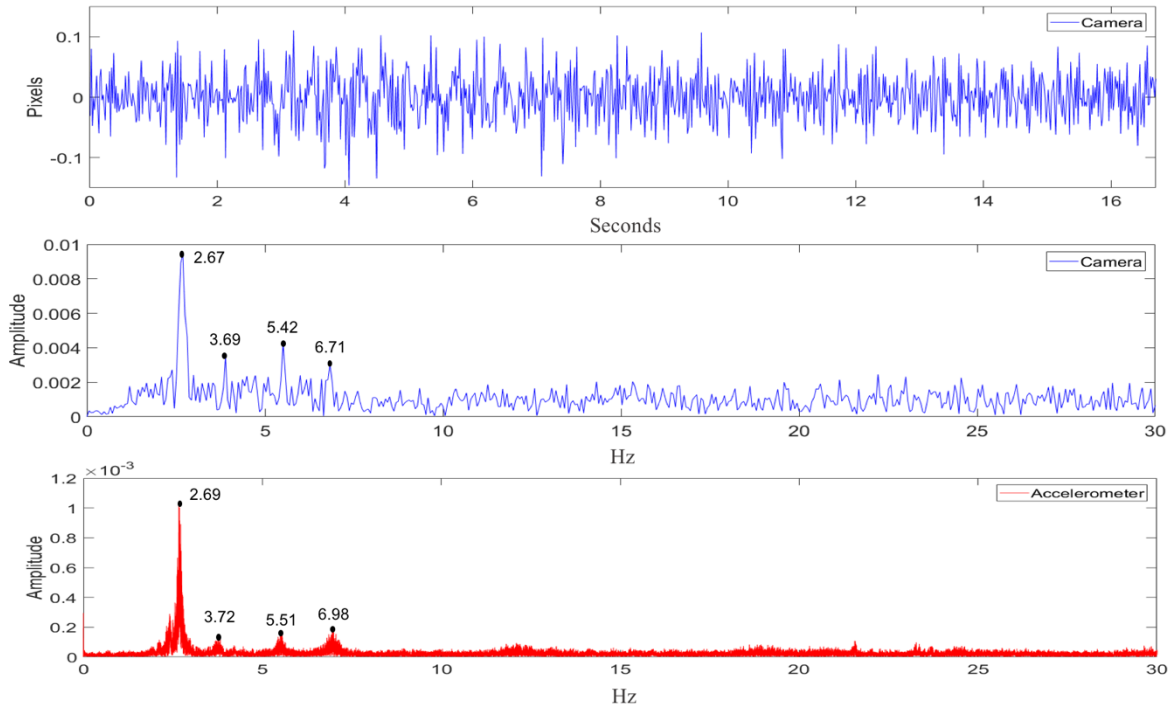

Figure 8 Comparison between camera and accelerometers. (Top): Displacement signal measured with camera; (Middle): Fourier spectrum of the camera measured signal and the identified first four modes; (Down): Fourier spectrum of the accelerometers measured signal and the identified first four modes

In Figure 9 (b) and (c), the edge mask and full field vibration map at the entire cropped camera view are presented. Similar as the laboratory test, the vibration map only chooses the strongest peak at each active pixel. Comparing to the indoor experiment, the scale of variation of the identified frequencies in the vibration map are much large. This can be caused by the environment-induced noises and the difference of structures' physical properties. It can be visualized that the resonant frequencies of most horizontal structures are located around 2.7 Hz which is coincident with the computed 1st mode in validation result. However, the resonant frequencies of some vertical structures are located around 3.7 Hz which closes to the computed 2nd mode (Table 1). Although there is no accelerometer located near the vertical structure that can validate this observation, the plausible result still shows the potential of using the proposed multi-point phase-based method for full field vibration measurement of complex structures.

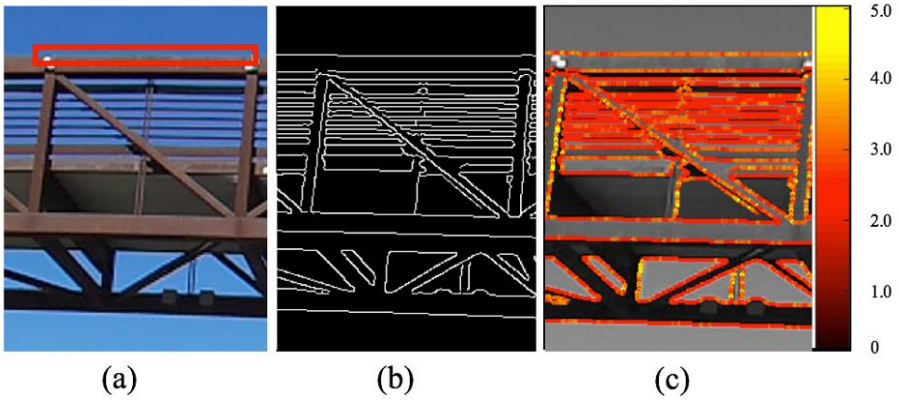

Figure 9 Pedestrian bridge (a) Cropped camera view with selected ROI (in red rectangle); (b) Edge mask; (c) Color-coded vibration map with color bar indicates the resonant frequencies

Railway Bridge

To visualize the ODS of multiple structures, the field experiment is implemented on an in-service rail truss bridge. A tripod stabilized video camera is positioned at one side of the bridge with distance nearly 10 meters to the middle spans of the bridge section. The location of camera and the camera view in the video are presented in Figure 11. A 10 seconds video that records the bridge vibration induced by a passing freight train is captured with the camera at the resolution of 1920×1080 and frame rate of 120 fps. Two bridge structures (S_1 and S_2) are explicitly chosen for vibration magnification where S_1 is a section of the main horizontal truss between two joints and S_2 is the upper part of a beam that connects the truss and floor deck of the rail bridge. Thus, instead of processing the entire images, the vibrations are only measured at active pixels located on S_1 and S_2. The pre-determined edge mask of S_1 and S_2 are respectively colored as shown in Figure 11 (b). Due to the environment noises and traffic, image enhancement is applied at the raw video sequences to increase the spatial contrast.

Figure 10 (a) Camera Location; (b) Image view of the railway bridge along with active pixels extracted at structure S_1 (in red) and S_2 (in blue)

The results of the identified means, standard deviations, and the select the constant ε for frequency band estimation are listed in Table 1. These parameters are identified by searching the strongest peaks in Fourier domain at all active pixels and estimated with the MLE. The ε is set to 1 as it will cover most of the individual peaks and, at the same time, avoid the overlap with peaks at other modes. The histogram of active pixels on S_1 and S_2 at each mode with the estimated parameters and probability density functions (PDF) of Gaussian distribution are demonstrated in Figure 11 and Figure 12. Figure 13 presents the average vibration signal in frequency domain with the frequency peaks and the estimated frequency bands of each structure. These frequency bands are then applied as the input to reconstruct the vibration magnified video with amplification factor set as 100. Snapshots of vibration magnified video cropped at S_1 and S_2 are respectively presented in Figure 14 and Figure 15. To better visualize the ODS, the active pixels in the original and amplified video are extracted and normalized to the range of $[-1,1]$ along the vibration direction. The comparison of these normalized active pixels at S_1 and S_2 with and without vibration magnification in video are shown in Figure 16 and Figure 17.

Table 1 Estimated mean ($\hat{\mu}$), standard deviation ($\hat{\sigma}$) and frequency band ($\widehat{fb}$) with the select ε for motion magnification

	Mode (k)	$\hat{\mu}$	$\hat{\sigma}$	ε	$\widehat{fb}$
Structure S_1	1	1.08	0.51	1	[0.57, 1.59]
	2	1.97	0.69	1	[1.28, 2.66]
	3	3.84	0.81	1	[3.03, 4.65]
Structure S_2	1	1.97	0.48	1	[1.49, 2.45]
	2	3.41	0.53	1	[2.88, 3.94]
	3	7.02	0.99	1	[6.03, 8.01]

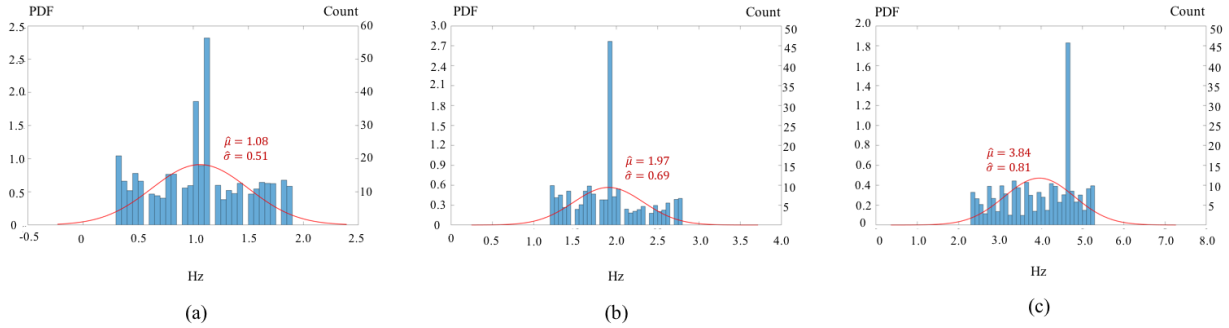

Figure 11 Histogram of modes and PDF of Gaussian distribution with the estimated mean and variance at S1: (a) Mode 1; (b) Mode 2; (c) Mode 3

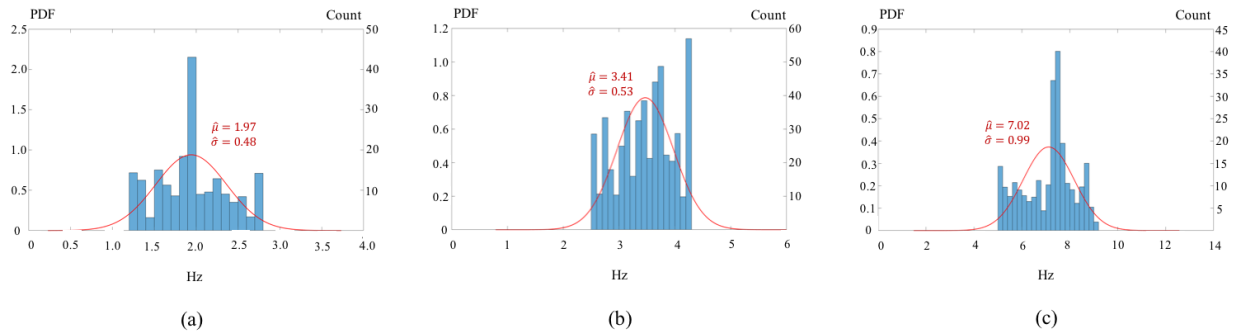

Figure 12 Histogram of modes and PDF of Gaussian distribution with the estimated mean and variance at S2: (a) Mode 1; (b) Mode 2; (c) Mode 3

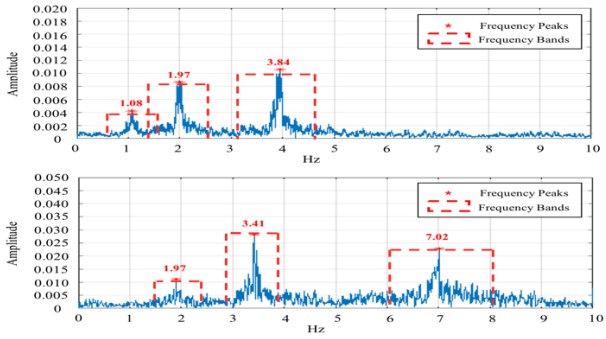

Figure 133 Fourier spectrum of averaged vibration frequency, frequency peaks and the estimated frequency bands of S_1 (Top) and S_2 (Down).

Figure 14 Snapshots of vibration magnified video of structure S_1 with amplified frequency bands at: (a) [0.57, 1.59]; (b) [1.28, 2.66]; (c) [3.03, 4.65]

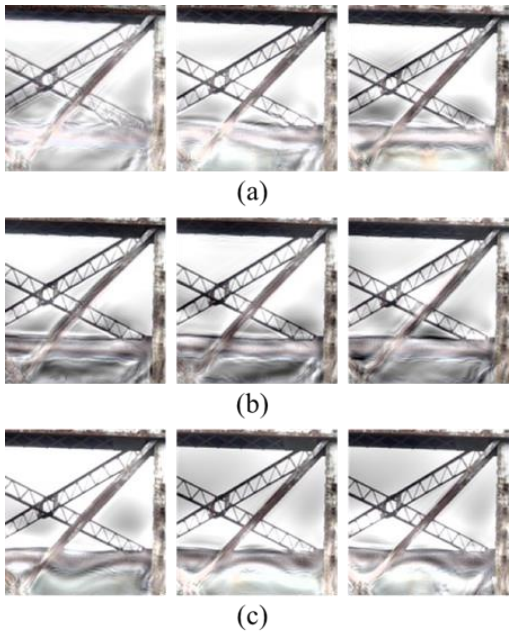

Figure 15 Snapshots of vibration magnified video at structure S_2 with amplified frequency bands at: (a) [1.49, 2.45]; (b) [2.88, 3.94]; (c) [6.03, 8.01]

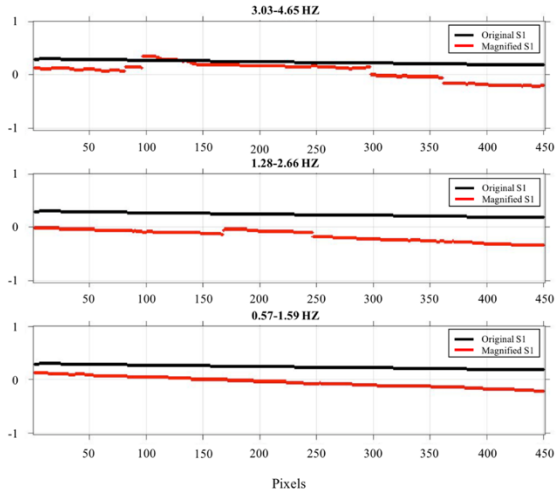

Figure 16 Vertical only normalized ODS of S_1 at the estimated frequency bands in original (black) and magnified (red) video

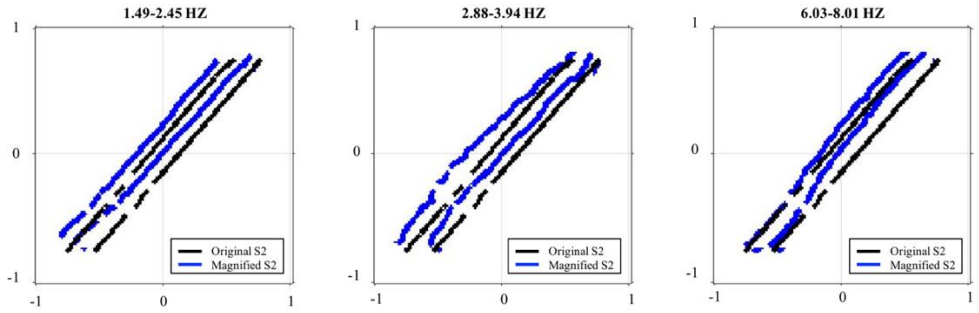

Figure 17 Horizontal and vertical both normalized ODS of S_2 at the estimated frequency bands in original (black) and magnified video (blue)

4. Conclusions

This research introduces a non-contact multi-point vibration measurement approach using the phase-based optical flow. The method can output a full-field vibration map for anomaly detection of complex structures. Comparing to the existing multi-point methods that relies on the intensity level changes, this method requires no surface preparations and can achieve sub-pixel accuracy even under outdoor environment. Specific noise reduction method is applied to increase the SNR and, at the same time, reserve the local motion variations at each pixel. Integrating the multi-point measurement result with the MLE, the magnified frequency bands can be estimated without human interaction as in the original motion magnification method, which increase the efficiency of mode magnification on complex structures. The proposed method is tested through both indoor laboratory experiment and outdoor field measurement.

There are several areas of this method can be further improved in the future study: First, this study only focus on the in-plane displacement with camera view perpendicular to the target structure. In practice, the vibrating structure contains both in-plane and out-of plane movement, which can be achieved by generating a three-dimensional vibration map. Second, the proposed method measures the pixel-wise vibration displacements. The structure torsion and twist, which requires to consider the relative motions of multiple motion signals, are not considered. Third, due to the dropped SNR, only the strongest peaks are used to generate the vibration map. Mode decomposition can be applied in the future to generate the clean vibration maps for all identified modes.

Reference

1. Doebling, S.W., C.R. Farrar, and M.B. Prime, *A summary review of vibration-based damage identification methods.* Shock and vibration digest, 1998. **30**(2): p. 91-105.

2. Sohn, H., et al., *A review of structural health review of structural health monitoring literature 1996-2001*. 2002, Los Alamos National Laboratory.

3. Nassif, H.H., M. Gindy, and J. Davis, *Comparison of laser Doppler vibrometer with contact sensors for monitoring bridge deflection and vibration.* Ndt & E International, 2005. **38**(3): p. 213-218.

4. Lee, J.J., et al., *Development and application of a vision-based displacement measurement system for structural health monitoring of civil structures.* Smart Structures and Systems, 2007. **3**(3): p. 373-384.

5. Pan, B., et al., *Two-dimensional digital image correlation for in-plane displacement and strain measurement: a review.* Measurement science and technology, 2009. **20**(6): p. 062001.

6. Ji, Y. and C. Chang, *Nontarget image-based technique for small cable vibration measurement.* Journal of Bridge Engineering, 2008. **13**(1): p. 34-42.

7. Carden, E.P. and P. Fanning, *Vibration based condition monitoring: a review.* Structural health monitoring, 2004. **3**(4): p. 355-377.

8. Lee, J.J. and M. Shinozuka, *A vision-based system for remote sensing of bridge displacement.* Ndt & E International, 2006. **39**(5): p. 425-431.

9. Ribeiro, D., et al., *Non-contact measurement of the dynamic displacement of railway bridges using an advanced video-based system.* Engineering Structures, 2014. **75**: p. 164-180.

10. Cigada, A., P. Mazzoleni, and E. Zappa, *Vibration monitoring of multiple bridge points by means of a unique vision-based measuring system.* Experimental Mechanics, 2014. **54**(2): p. 255-271.

11. Kim, S.-W. and N.-S. Kim, *Dynamic characteristics of suspension bridge hanger cables using digital image processing.* NDT & E International, 2013. **59**: p. 25-33.

12. Guo, J., *Dynamic displacement measurement of large-scale structures based on the Lucas–Kanade template tracking algorithm.* Mechanical Systems and Signal Processing, 2016. **66**: p. 425-436.

13. Horn, B.K. and B.G. Schunck, *Determining optical flow.* Artificial intelligence, 1981. **17**(1-3): p. 185-203.

14. Caetano, E., S. Silva, and J. Bateira, *A vision system for vibration monitoring of civil engineering structures.* Experimental Techniques, 2011. **35**(4): p. 74-82.

15. Schumacher, T. and A. Shariati, *Monitoring of structures and mechanical systems using virtual visual sensors for video analysis: Fundamental concept and proof of feasibility.* Sensors, 2013. **13**(12): p. 16551-16564.

16. Song, Y.-Z., et al., *Virtual visual sensors and their application in structural health monitoring.* Structural Health Monitoring, 2014. **13**(3): p. 251-264.

17. Shariati, A. and T. Schumacher, *Eulerian-based virtual visual sensors to measure dynamic displacements of structures.* Structural Control and Health Monitoring, 2016.

18. Wu, H.-Y., et al., *Eulerian video magnification for revealing subtle changes in the world.* 2012.

19. Wadhwa, N., et al., *Phase-based video motion processing.* ACM Transactions on Graphics (TOG), 2013. **32**(4): p. 80.

20. Gautama, T. and M. Van Hulle, *A phase-based approach to the estimation of the optical flow field using spatial filtering.* IEEE Transactions on Neural Networks, 2002. **13**(5): p. 1127-1136.

21. Chen, J.G., et al., *Modal identification of simple structures with high-speed video using motion magnification.* Journal of Sound and Vibration, 2015. **345**: p. 58-71.

22. Chen, J.G., et al., *Developments with motion magnification for structural modal identification through camera video*, in *Dynamics of Civil Structures, Volume 2*. 2015, Springer. p. 49-57.

23. Diamond, D., P. Heyns, and A. Oberholster, *Accuracy evaluation of sub-pixel structural vibration measurements through optical flow analysis of a video sequence.* Measurement, 2017. **95**: p. 166-172.

24. Yang, Y., et al., *Blind identification of full-field vibration modes from video measurements with phase-based video motion magnification.* Mechanical Systems and Signal Processing, 2017. **85**: p. 567-590.

25. Sarrafi, A., et al., *Vibration-based damage detection in wind turbine blades using Phase-based Motion Estimation and motion magnification.* Journal of Sound and Vibration, 2018. **421**: p. 300-318.

26. Mas, D., et al., *Methods and algorithms for video-based multi-point frequency measuring and mapping.* Measurement, 2016. **85**: p. 164-174.

27. Fleet, D.J. and A.D. Jepson, *Computation of component image velocity from local phase information.* International journal of computer vision, 1990. **5**(1): p. 77-104.

28. Freeman, W.T. and E.H. Adelson, *The design and use of steerable filters.* IEEE Transactions on Pattern analysis and machine intelligence, 1991. **13**(9): p. 891-906.

29. Jain, A.K., *Fundamentals of digital image processing*. 1989: Prentice-Hall, Inc.

30. Brincker, R., L. Zhang, and P. Andersen, *Modal identification of output-only systems using frequency domain decomposition.* Smart materials and structures, 2001. **10**(3): p. 441.

31. Myung, I.J., *Tutorial on maximum likelihood estimation.* Journal of mathematical Psychology, 2003. **47**(1): p. 90-100.